RSC Advances

PAPER

View Article Online
View Journal | View Issue

CrossMark click for updates

Cite this: *RSC Adv.*, 2015, **5**, 42721

Low temperature direct bonding of silica glass *via* wet chemical surface activation†

Chengle Mai,[a] Mingyu Li*[a] and Shihua Yang[b]

Received 14th April 2015
Accepted 6th May 2015

DOI: 10.1039/c5ra06705g

www.rsc.org/advances

Silica glass pairs were directly bonded by wet chemical surface activation at a low temperature. A smooth joint interface with no voids and micro cracks was obtained with the assistance of a 250 °C heat treatment and a pressure of ~30 MPa, and the excellent transmittance of the bonded pair was demonstrated by UV-Vis absorptions. This new method can tolerate a silica glass surface roughness as high as 6 nm. A demo chip with a microfluidic channel was also prepared by this method. A modified model for the glass-to-glass bonding mechanism is proposed based on the surface and interface characterization. Raman scattering analysis showed that Si–O–Si linkages at the silica glass surface were broken, and colloid-like hydrolyzed layers formed on the glass surface after the activation treatment. TEM and EELS results revealed that the 3D glass structure of the Si–O–Si linkages formed again at the interface of the directly bonded silica glass pairs after low-temperature annealing.

Introduction

Silica glass is an ideal substrate material for fabricating microfluidic chips because of its excellent properties, such as its high physical rigidity, chemical inertness, high thermal stability, and excellent transparency. However, as the critical step in the manufacturing of glass microchips, the bonding technology for glass pairs impedes the applications and development of microfluidic chips.[1] Although wafer bonding technology has been rapidly developed in response to an increased demand in the development of 3D packages of integrated circuits (ICs) and the heterogeneous integration of micro-electro-mechanical systems (MEMS),[2–5] the development of a method for bonding a glass wafer robustly, conveniently and at low cost is highly desirable.

In the last decade, wafer boding has been developed in two main directions, *i.e.*, intermediate and direct bonding.[6] Comparatively, direct bonding is advantageous in bonding silica-based glass while retaining the properties of the rare materials, such as their optical properties. A variety of methods for glass-to-glass direct bonding have been developed.[7,8] Among them, fusion bonding is the most widely used method in commercial manufacturing. However, this method is usually performed at extremely high temperatures (approximately 1000 °C) for silica glass. Therefore, functional elements cannot be integrated in this conventional bonding method. Techniques enabling glass-to-glass direct bonding at low temperatures are more attractive.

At present, some research organizations use the plasma-activated direct bonding method to bond glass and silicon wafers.[9–14] Smooth interfaces have been obtained with this method, even at room temperature. However, it requires more rigorous conditions than the traditional fusion bonding method. For example, the sample surfaces must be very smooth (root mean square roughness < 0.5 nm), and all processes must be performed under ultra-high vacuum in a clean room (1000 class).[15] Anodic bonding can also bond the glass pairs at low temperature, but it requires a nano-adhesive layer plating on the glass surface, which may deteriorate the glass' optical properties.[16–18] In this study, we report a low-temperature wet chemical surface activation bonding method to directly bond silica glass pairs, and propose a modified model for glass-to-glass bonding mechanism. This new method can be performed in a routine laboratory without an ultra-high-vacuum system and clean room.

Experimental section

Materials

For silica glass bonding pairs, 10 mm × 10 mm and 30 mm × 15 mm double-surface-polished silica glass pieces with a thickness of approximately 1 or 2 mm were used. For glass-to-silicon bonding pairs (used to investigate additional details of the bonding mechanism), 10 mm × 10 mm single-surface-polished (100)-oriented silicon pieces with a 500 μm thickness were used. The surface roughness of the samples was as high as 6 nm. For demo devices fabrication, we used 5 mm ×

[a]State Key Laboratory of Advanced Welding and Joining, Harbin Institute of Technology Shenzhen Graduate School, Shenzhen, 518055, People's Republic of China. E-mail: myli@hit.edu.cn; Tel: +86-755-26033463

[b]Shanghai Aerospace Equipments Manufacturer, Shanghai, 200245, People's Republic of China

† Electronic supplementary information (ESI) available: Fig. S1 and S2; movie 1 and 2. See DOI: 10.1039/c5ra06705g

5 mm × 2 mm and 0.2 mm × 2.4 mm × 5 mm polished silica glass pieces.

Bonding procedure

Cleaning process. Before the activation treatment, all samples were initially passed through a proprietary multistage bath cleaning process. First, the glass pieces were rinsed in acetone and methanol with ultrasonic assistance for 8 min each. The sample pieces were then cleaned in a sulfuric acid (H_2SO_4)/hydrogen peroxide (H_2O_2) mixture (SPM) ($H_2SO_4 : H_2O_2 = 4 : 1$) at 120 °C for 15 min. Finally, the sample pieces were boiled in standard RCA-1 ($NH_4OH : H_2O_2 : H_2O = 1 : 1 : 5$) and RCA-2 ($HCl : H_2O_2 : H_2O = 1 : 1 : 5$) solutions at 100 °C for 15 min, respectively. Notably, during the intervals of these steps, all samples were continuously rinsed in deionized water (DI water) to prevent secondary contamination.

Surface activation treatment. The samples were rinsed in the activation solution ($NH_4OH : H_2O_2 : H_2O = 6 : 1 : 3$) at 80 °C for 30 min. Notably, during each process, we carefully washed the samples under running DI water to remove any residue from the previous procedure and then kept the samples in DI water for the next procedure.

Pre-bonding. The surfaces of the samples were washed with running DI water for 5 min. The samples were then carefully aligned and contacted directly with each other in DI water. Subsequently, the combined pieces were dried and loaded into a vacuum drying oven (DZF-6020). The oven was then evacuated to 120 Pa and maintained at 100 °C for 2 h to complete the pre-bonding process.

Annealing bonding. Finally, the samples were placed into a stainless steel jig that was designed for applying pressure (5–30 MPa). The jig was kept in a vacuum drying chamber for 2–10 h to complete the low-temperature annealing bonding at 100–250 °C.

Bonding strength evaluation

The bonding strength was measured using a tensile pulling tester with a pulling speed of 0.05 mm min^{-1}. The bonded specimens were glued with stainless steel jigs clamping to the fixture of the pulling tester.

Chip fabrication

A demo chip was fabricated by the 3D stacking mode using the bonding procedure above. A steel wire with a diameter of ~200 μm was set between the two thin glass pieces in the stack to define the size of the microfluidic channel (Fig. 1). We could obtain a microfluidic channel with a polished surface using this method.

Leakage test

To evaluate the maximum pressure that the bonding parts can take without leakage, we designed an experimental setup for dead-end leakage test (Fig. S1†). One end of the device was glued to a steel jig interconnecting to the pressurized water tank, which was connected to the compressed nitrogen bottle with gas flow regulator. The dyed water in the water tank was injected into the channel under the pressure applied (ESI movie 1†). For achieving the dead-end design of the channel, we blocked the other end of the channel with rubber. While adjusting the gas flow regulator, the applied pressure increases slowly to the expected value.

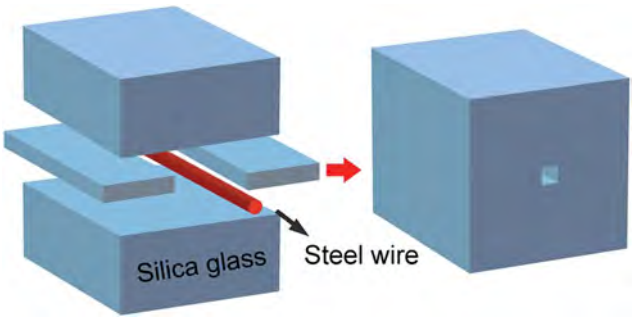

Fig. 1 Schematic image of the demo chip fabrication bonding process.

Characterization

The roughness of the samples was measured using atomic force microscopy (AFM, CSPM5500). The surface chemistry of the glass was examined by Raman scattering. The thickness of the silicon oxide layer on silicon was measured by ellipsometry (M2000UI, J. A. Woollam Co., Inc.). The transmittance of the bonded pairs was examined using UV-Vis spectrophotometry (SHIMADZU UV-2600). Silica glass samples with a thickness of 4 mm were also measured for comparison with the boned pairs. The bonding interfaces were examined by scanning electron microscopy (SEM), high-resolution transmission electron microscopy (HRTEM), Z-contrast scanning TEM (STEM) and electron energy-loss spectroscopy (EELS). TEM observations and EELS analyses were performed on a Tecnai G2 F20 device equipped with a Gatan GIF Quantum 963 energy filter. Cross-sectional TEM samples were prepared using a standard focused ion beam (FIB) procedure (FEI Helios NanoLab 600).

Results and discussion

Surface roughness and surface chemistry

The surface of the silica glass after the activation treatment (Fig. 2b) was as smooth as that before the treatment (Fig. 2a), with a surface roughness of approximately 6 nm. This result also indicates that our bonding process tolerates a high surface roughness of up to 6 nm. In the case of the silicon, the ellipsometry results showed that the thickness of the oxide layer (~2.2 nm) was not affected by the activation treatment.

Before the wet surface activation treatment, the Raman shift of the sample surface (Fig. 2c) was consistent with the standard spectrum of silica glass. The standard Raman spectrum of fused silica exhibits six characteristic peaks (430, 490, 600, 800, 1060 and 1200 cm^{-1}).[19] The peak at 430 cm^{-1} is attributed to the stretching-bending vibration of the Si–O–Si bridges in large silicate rings. The peaks at 485 and 600 cm^{-1} are known as

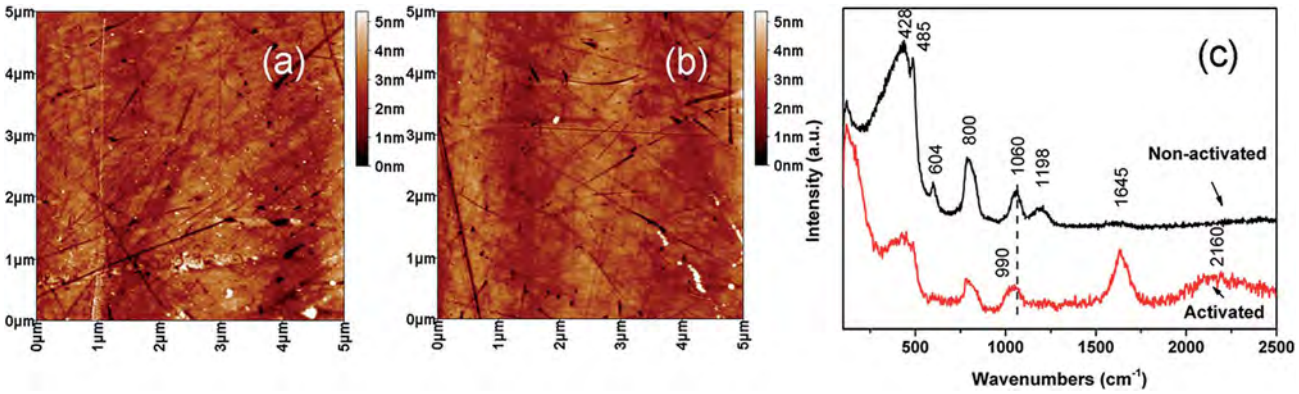

Fig. 2 AFM topographic surface images of the glass surface (a) before and (b) after the wet chemical activation treatment. (c) Raman shift of the glass sample surface before and after the activation treatment.

defect lines, which refer to the breathing modes of four- and three-membered silicate rings, respectively.[20] The peak at 800 cm^{-1} is due to Si–O–Si bending. Two bands at approximately 1060 and 1200 cm^{-1} are attributed to the asymmetric stretching of Si–O–Si bridges in the silica glass network.[21]

After the activation treatment, the glass surface became hydrophilic. We observed a fresh band at approximately 990 cm^{-1} (Fig. 2c), which is attributed to the surface Si–OH groups.[22] Meanwhile, the intensities of the 430, 490, 800, and 1060 cm^{-1} peaks decreased, and the initially observed bands at approximately 600 cm^{-1} and 1200 cm^{-1} almost completely disappeared. In addition, two fresh peaks appeared at approximately 1645 cm^{-1} and 2160 cm^{-1}. The peak at approximately 1645 cm^{-1} was due to the H_2O vibration mode, whereas the peak at approximately 2160 cm^{-1} was the overtone of 980 cm^{-1} and the higher wavenumber of 3690 cm^{-1}. The band at 3690 cm^{-1} (outside the scope of our recorded spectra) was due to the –OH stretching vibration of water.[23] These results can be explained by the breakage of silicate rings and the formation of Si–OH (please refer to the mechanism discussion for more details).

Transmission spectra

Two exemplary recorded UV-Vis transmission spectra of glass samples are displayed in Fig. 3. No significant difference was observed between the spectrum of the bonded pairs and that of the bulk glass with the same thickness. The bonded pair exhibited excellent transmittance as well as the bulk, which suggests that no deterioration occurred in the joint interface after the bonding process. Moreover, the absorbed peak at approximately 240 nm, which is due to the oxygen vacancy,[24] disappeared after the bonding process because both the surrounding strong oxidizing liquid and diffusion of the hydroxyl groups can fill the oxygen vacancy in the network of the silica glass.

Interface characterizations

SEM. Perfect bonding requires contaminant-free conditions. The observation of Newton rings indicates bad bonding samples.[25] We examined the interface around the Newton rings of a sample by SEM, as shown in Fig. 4a. Obviously, the interface near the center of the Newton rings was not tightly bonded. The opening at the interface narrowed gradually along the radius direction (Fig. 4b–d). Through optimizing the process, we ensure that no Newton rings appeared in our samples prepared for the investigations. We achieved the highest bonding strength (4.5 MPa) at 250 °C annealing for 10 h under the assistance of pressure of ~30 MPa. The samples we used for interface analysis are prepared in the condition mentioned above. Fig. 4e shows an optical picture of a silica glass chip with a ~200 μm rectangular microfluidic channel bonded through the low temperature wet chemical surface activation direct bonding process. Red dye was injected into the capillaries, and no liquid leakage was observed in the microfluidic chip, indicating hermetic sealing in this structured areas. Leakage test results of the dead-end design showed that the channel can withstand pressure up to ~500 kPa without any leakage (Fig. S2 and ESI movie 2†). The cross-sectional SEM image of the rectangle microfluidic channel of the bonded chip is presented in Fig. 4f. The bonding interface can barely be distinguished by SEM.

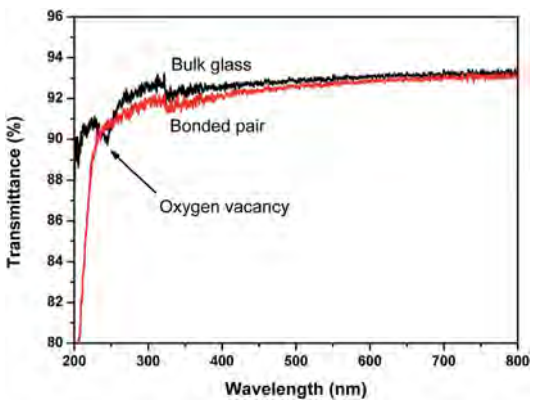

Fig. 3 UV-Vis transmission spectra of the bulk glass and glass bonded pairs.

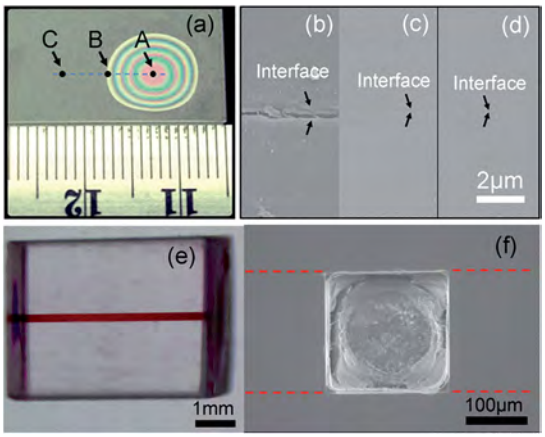

Fig. 4 (a) Optical top view graphic of the Newton rings in the glass pairs. (b), (c) and (d) Cross-sectional SEM image of the bonding interface around the points marked A, B and C in (a). The relative arrow pairs indicate the location of the interface in (b), (c) and (d). (e) Optical top view of the demo chip with a rectangular microfluidic channel. (f) Cross-sectional SEM image of the rectangular microfluidic channel. The red dashed lines in (f) indicate the interface.

TEM. The STEM image of the cross-sectional interface of the glass-to-glass pair is shown in Fig. 5a. Ga^+ ions remaining from the Ga^+ source of FIB segregate at the bonding interface; therefore, we can easily identify the interface using the STEM mode. Core-loss EELS spectra of Si-$L_{2,3}$ and O-K collected from the interface and the bulk were both recorded (Fig. 5b and c). We observed little change between the EELS spectra obtained from the interface and those obtained from the bulk fused glass, indicating that the microstructure of the bonding interface was almost the same as that of the bulk glass.

For a detailed investigation of the bonding mechanism, we also studied the glass-to-silicon pair bonding interface. This bonding mechanism is reasonably assumed to be the same as that of the glass-to-glass bonding pairs because they are both

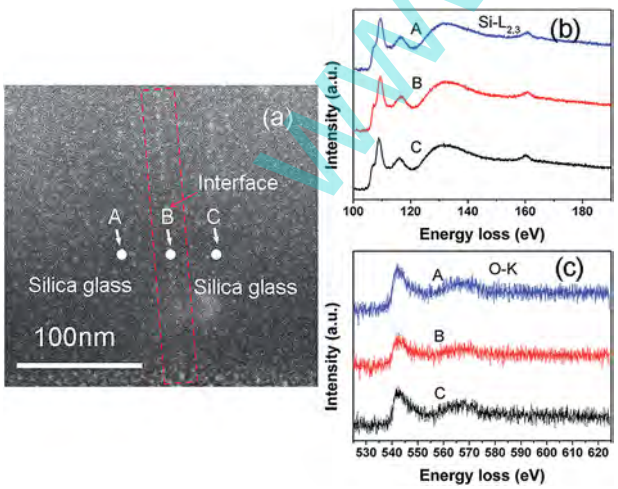

Fig. 5 (a) Cross-sectional STEM image of the interface of the glass bonded pair. (b) and (c) Si-$L_{2,3}$ and O-K edge EELS spectra collected from points A, B and C marked in (a).

SiO_2-to-SiO_2 joints. On the basis of the HRTEM images (Fig. 6a) of the bonding interface, we conclude that the interface is as smooth as that obtained from anodic bonding[26] or the plasma activation method.[9] We can also disturb the silicon oxide layer (~2 nm thickness) on the silicon surface, whose thickness coincided with the result we observed by ellipsometry. In addition to this oxide layer, another amorphous layer (3–4 nm thickness), which exhibited lower contrast than the neighboring layer, was also present. This layer was part of the bonding interface.

We performed an EELS line scan across the interface (Fig. 6b). Both the Si-$L_{2,3}$ and O-K edge spectra were recorded with a separation of approximately 1 nm between each spectrum (Fig. 6d and e). We can discern the transition of the Si-$L_{2,3}$ edge spectra along the interface (silicon → silicon oxide → interface → silica glass). The Si edge shifts from 102 eV in silicon to 108 eV in silica glass consequent to the different energies of different Si bonds. By contrast, the O edge appears gradually because no O was present in the silicon bulk. Consistent with the results obtained from the interface of glass bonds, no significant change was observed in either the Si-$L_{2,3}$ or the O-K edge spectra collected around the bonding interface of the silicon-to-glass bonded pairs.

More details regarding the EELS analysis provided the quantitative profile of the O/Si concentration ratios across the interface (Fig. 6c). We quantified all EELS spectra according to the method described in ref. 27. From the ratio profile, we observed that the O/Si ratio around the bonding interface (~1.3) was lower than that in the glass bulk (~2.0). A slow transition of the ratio from the interface region to the silica bulk was observed. However, from the silicon region to the oxide layer, the slope of the profile changed substantially, indicating the transition of the Si/SiO_x interface on the silicon surface.

Bonding mechanism

Although some models have been developed for the mechanism of silicon wafer direct bonding,[28–30] details regarding the microstructure of the activated glass surface and the evolution of the bonded interface are still poorly understood. On the basis of our experiment results, we propose an updated model for wet chemical surface activation silica glass direct bonding.

The networks of silica glass consist of $[SiO_4]^{4-}$ tetrahedral units linked at their corners by bridging Si–O–Si bonds.[31] The fresh surface of the silica glass contains dangling bonds (≡Si–$^+$ and –O–$^-$) as exhibited in Fig. 7a. During the cleaning process, hydroxyl groups (–OH) and amino groups (–NH_2) can be adsorbed by these dangling bonds. In the activation treatment, more silicate rings on the glass surface are broken because of reaction (1) (Fig. 7), then more activated groups (–OH and –NH_2) are attached to the Si atoms. This process is substantiated by Raman spectra (Fig. 2c). The intensity decreases of the 430 and 490 cm^{-1} peaks and the disappearance of the 600 and 1200 cm^{-1} peaks indicated the breakages of silicate rings. The fresh peak related to Si–OH at approximately 980 cm^{-1} shifting to 990 cm^{-1} confirmed both the exhibit of the weak hydrogen bonded Si–OH and the existence of Si–NH_2 on the surface.[32]

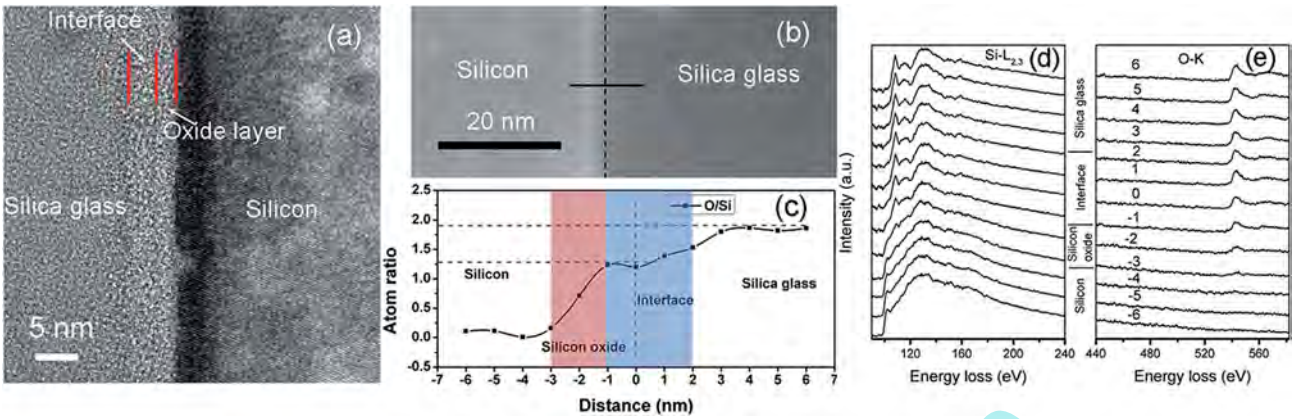

Fig. 6 (a) Cross-sectional HRTEM image of the silicon-to-glass bonding pair; the red lines indicate the bonding interface and oxide layer on silicon. (b) STEM image of the interface; the horizontal line indicates the EELS line-scan position, and the vertical dashed line indicates the bonding interface. (c) Profile of the O/Si ratio as measured using EELS and the EEL spectra recorded along the scan line containing (d) Si-$L_{2,3}$ and (e) O-K edges. The interface is denoted as 0, the silicon side is indicated by negative numbers, and the glass side is indicated by positive numbers.

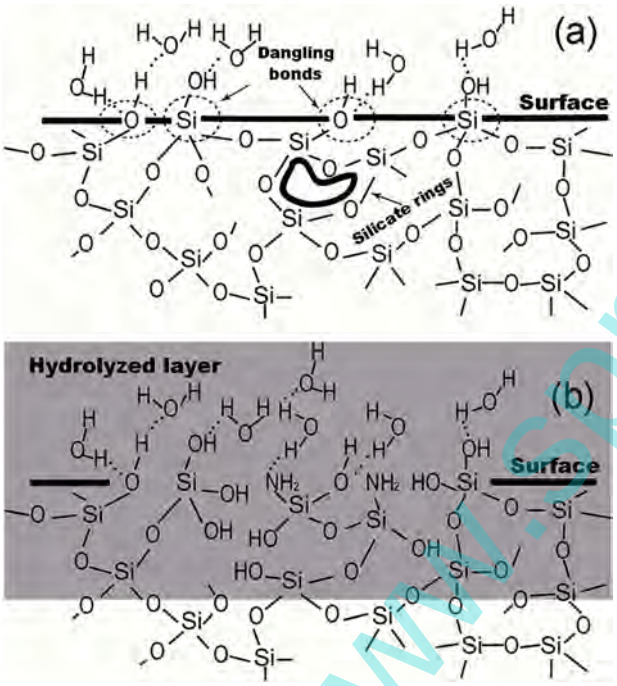

Fig. 7 (a) Schematics of the non-activated glass surface; the dark straight line indicates the glass surface, the dark curve marks the three-membered silicate rings, and dashed rings indicate the dangling bonds. (b) Schematics of the activated glass surface and the formation of the hydrolyzed layer. The dark region indicates the hydrolyzed layer.

$$2(\text{Si–O–Si}) + NH_4OH \rightarrow \text{Si–}NH_2 + 3(\text{Si–OH}) \quad (1)$$

As reaction (1) progresses, numerous activated groups are attached to the glass surface. Then, the surface is activated and becomes hydrophilic. H_2O molecules can be adsorbed by the hydrogen bond, which is supported by a Raman shift at approximately 1645 cm^{-1} (Fig. 2c). Finally, one colloid-like, hydrolyzed layer would uniformly form on the glass surface (Fig. 7b and 8a). These layers gain nanometer thickness with lower viscosity than the bulk and contain a high density of –OH and H_2O similar to Ludox®.

During the pre-bonding process, both –OH and $–NH_2$ can react with each other to form Si–O–Si linkage (reactions (2), (3) and (4)) with concomitant removal of small molecules (H_2O, NH_3 and H_2) from the interface, and the surfaces become closer. Reaction (4) is less likely to occur because more hydroxyl groups are generated than amino groups.

$$\text{Si–OH} + \text{HO–Si} \rightarrow \text{Si–O–Si} + \text{HOH} \quad (2)$$

$$\text{Si–}NH_2 + \text{OH–Si} \rightarrow \text{Si–O–Si} + NH_3 \quad (3)$$

$$\text{Si–}NH_2 + NH_2\text{–Si} \rightarrow \text{Si–N–N–Si} + 2H_2 \quad (4)$$

The transformation of two neighboring silanol bonds into siloxane is an exothermal process.[33] These transformations spontaneously occur during the pre-bonding process. However, they only lead to a small fraction of adhesion (Fig. 8b). Some nanogaps were left in the interface (Fig. 8c). The surface of these nanogaps still possesses unbound activated surface groups.

The surface bonding can be strengthened by closing all these nanogaps. However, the process then becomes endothermic because of the obvious spatial restrictions from the neighboring siloxane bonds.[33] Therefore, additional amounts of energy are required. We applied low-temperature annealing (250 °C) and pressure of ~30 MPa to achieve this process. The nanogaps are closed when the local deformation of the hydrolyzed layer occurs and the remaining surface groups react with their neighboring groups. This process appears to be the inverse of stress corrosion.[34] Simultaneously, the products such as H_2O, NH_3 and H_2 slowly diffused away through the not-fully-dehydrated layer or diffused into the bulk, filling the oxygen vacancies. This occurrence of this process is supported by the UV-Vis transmission spectra (Fig. 3). When the condensation-polymerization of the hydrolyzed layers was completed, a smooth bonded interface was obtained. As a newly formed

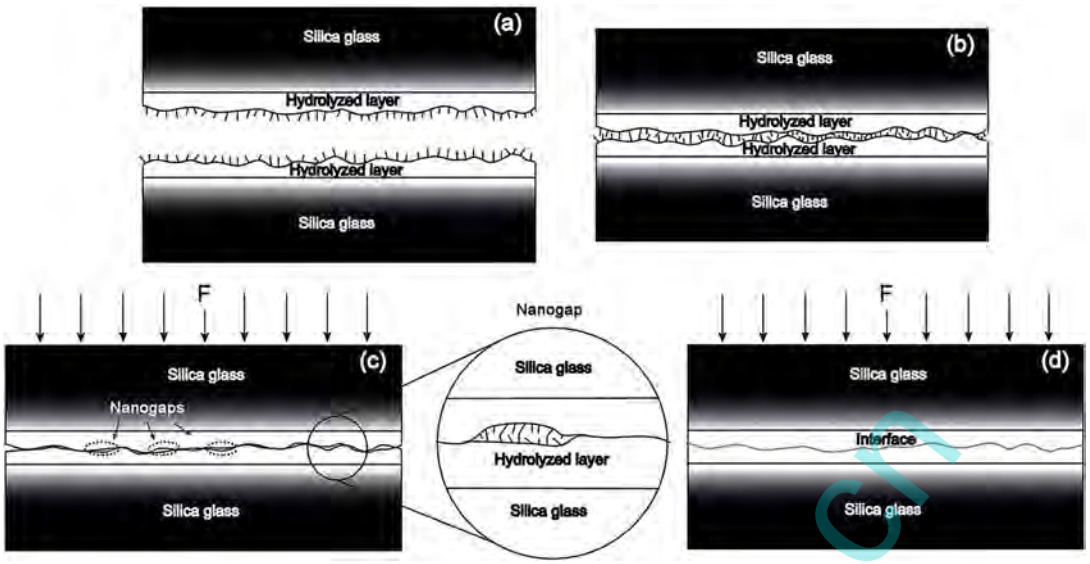

Fig. 8 Schematics of the bonding mechanism, as follows: (a) the activated glass surface, (b) the bonding interface after the pre-bonding process, and (c) interface of the bonding pair during pressure-assisted annealing at 250 °C. (d) Schematic of the bonded glass pair after annealing. The dashed lines in (c) point to the nanogaps at the interface. The schematic of the partial enlargement in (c) indicates the surface condition of the nanogap. The short line in the image represents the surface groups –OH and $-NH_2$. The connected short lines in (b) and (c) represent the Si–O–Si linkages.

layer, the network density of the interface might be lower than that of the bulk, which coincides with the ratio profile obtained by EELS analysis (Fig. 6c).

In summary, the mechanism (Fig. 8) we proposed consists of three stages: (1) the network of the glass surface breaks, and hydrolyzed layers form on the glass surface after the activation treatment; (2) during pre-bonding, a small fraction of adhesion is achieved, and nanogaps with unbound activated surface groups remain; and (3) during low-temperature annealing, the interfaces gradually dehydrate, forming the 3D glass structure of Si–O–Si linkages and terminating with condensation-polymerization.

Conclusions

In conclusion, we developed a low-temperature surface activation method to directly bond silica glass pairs. This method avoids the strict requirements, such as ultrahigh vacuum, a clean room and extremely high temperatures, all of which are required in conventional fusion bonding or the plasma activation method. We found that as long as the hydration layer could be uniformly generated on the surface of the glass, we could obtain a smooth bonding interface if the roughness satisfies our requirement (<6 nm). A demo chip with a ~200 μm microfluidic channel can also be fabricated by this method. This technique will significantly influence the fabrication process of silica glass microfluidic chips. Microfluidic chips with a regularly shaped, smooth surface capillary pipe can be fabricated with the 3D stacking bonding mode through this method. The procedures for preparing a microfluidic chip with a capillary pipe, without using the photolithographic and wet chemical etching techniques, have now become possible. Our studies will accelerate research on microfluidic systems and the application of glass microfluidic chips.

Acknowledgements

The authors thank Prof. He Kejian and Dr Yan Ning at the Modern Analysis and Testing Center of CSU for their support and discussion of the TEM observations and EELS analysis results. We thank Lv Shilong for his assistance with the preparation of the TEM sample by FIB.

Notes and references

1 Y. Xu, C. Wang, L. Li, N. Matsumoto, K. Jang, Y. Dong, K. Mawatari, T. Suga and T. Kitamori, *Lab Chip*, 2013, **13**, 1048.
2 J. B. Lasky, *Appl. Phys. Lett.*, 1986, **48**, 78.
3 M. Shimbo, K. Furukawa, K. Fukuda and K. Tanzawa, *J. Appl. Phys.*, 1986, **60**, 2987.
4 Q. Tong and U. M. Gösele, *Adv. Mater.*, 1999, **11**, 1409.
5 K. Y. Byun, I. Ferain, P. Fleming, M. Morris, M. Goorsky and C. Colinge, *Appl. Phys. Lett.*, 2010, **96**, 102110.
6 R. Arayanarakool, S. Le Gac and A. van den Berg, *Lab Chip*, 2010, **10**, 2115.
7 Y. Akiyama, K. Morishima, A. Kogi, Y. Kikutani, M. Tokeshi and T. Kitamori, *Electrophoresis*, 2007, **28**, 994.
8 Y. Xu, C. Wang, Y. Dong, L. Li, K. Jang, K. Mawatari, T. Suga and T. Kitamori, *Anal. Bioanal. Chem.*, 2012, **402**, 1011.
9 M. Howlader, M. G. Kibria, F. Zhang and M. J. Kim, *Talanta*, 2010, **82**, 508.
10 J. Lee, A. Ali, K. Kim, J. Kim, D. Choi, J. Choi and J. Jeong, *J. Micromech. Microeng.*, 2010, **20**, 45005.

11 S. Queste, R. Salut, S. Clatot, J. Rauch and C. G. K. Malek, *Microsyst. Technol.*, 2010, **16**, 1485.
12 C. Sabbione, L. Di Cioccio, L. Vandroux, J. Nieto and F. Rieutord, *J. Appl. Phys.*, 2012, **112**, 63501.
13 A. Shigetou and T. Suga, *J. Electron. Mater.*, 2012, **41**, 2274–2280.
14 C. Wang and T. Suga, *Microelectron. Reliab.*, 2012, **52**, 347.
15 M. Howlader, H. Okada, T. H. Kim, T. Itoh and T. Suga, *J. Electrochem. Soc.*, 2004, **151**, G461.
16 W. Yen and Y. Lin, *J. Adhes. Sci. Technol.*, 2009, **23**, 151.
17 V. G. Kutchoukov, F. Laugere, W. van Der Vlist, L. Pakula, Y. Garini and A. Bossche, *Sens. Actuators, A*, 2004, **114**, 521.
18 A. Berthold, L. Nicola, P. M. Sarro and M. J. Vellekoop, *Sens. Actuators, A*, 2000, **82**, 224.
19 G. E. Walrafen and P. N. Krishnan, *J. Chem. Phys.*, 1981, **74**, 5328.
20 A. Pasquarello and R. Car, *Phys. Rev. Lett.*, 1998, **80**, 5145.
21 A. Winterstein-Beckmann, D. M. Ncke, D. Palles, E. I. Kamitsos and L. Wondraczek, *J. Non-Cryst. Solids*, 2014, **401**, 110.
22 S. Agnello, D. Di Francesca, A. Alessi, G. Iovino, M. Cannas, S. Girard, A. Boukenter and Y. Ouerdane, *J. Appl. Phys.*, 2013, **114**, 104305.
23 R. H. Stolen and G. E. Walrafen, *J. Chem. Phys.*, 1976, **64**, 2623.
24 M. Tomozawa, H. Li and K. M. Davis, *J. Non-Cryst. Solids*, 1994, **179**, 162.
25 B. Renberg, K. Sato, T. Tsukahara, K. Mawatari and T. Kitamori, *Microchim. Acta*, 2009, **166**, 177.
26 Q. F. Xing, M. Yoshida and G. Sasaki, *Scr. Mater.*, 2002, **47**, 577.
27 T. Zheleva, A. Lelis, G. Duscher, F. Liu, I. Levin and M. Das, *Appl. Phys. Lett.*, 2008, **93**, 22108.
28 Y. Backlund, K. Ljungberg and A. Soderbarg, *J. Micromech. Microeng.*, 1992, **2**, 158.
29 C. Ventosa, C. Morales, L. Libralesso, F. Fournel, A. M. Papon, D. Lafond, H. Moriceau, J. D. Penot and F. Rieutord, *Electrochem. Solid-State Lett.*, 2009, **12**, H373.
30 T. Plach, K. Hingerl, S. Tollabimazraehno, G. Hesser, V. Dragoi and M. Wimplinger, *J. Appl. Phys.*, 2013, **113**, 94905.
31 P. F. McMillan, B. T. Poe, P. Gillet and B. Reynard, *Geochim. Cosmochim. Acta*, 1994, **58**, 3653.
32 C. A. Murray and T. J. Greytak, *J. Chem. Phys.*, 1979, **71**, 3355.
33 O. Lichtenberger and J. Woltersdorf, *Mater. Chem. Phys.*, 1996, **44**, 222.
34 T. A. Michalske and S. W. Freiman, *J. Am. Ceram. Soc.*, 1983, **66**, 284.